Multidrug cocrystal of anticonvulsants: Influence of strong intermolecular interactions on physiochemical properties

Ramanpreet Kaur,[a] *Katie L. Cavanagh,*[b] *Naír Rodríguez-Hornedo,* [b] *and Adam J. Matzger**[ac]

[a] Department of Chemistry, University of Michigan, Ann Arbor, Michigan, USA

[b] Department of Pharmaceutical Sciences, University of Michigan, Ann Arbor, Michigan, USA

[c] Macromolecular Science and Engineering, University of Michigan, Ann Arbor, Michigan, USA

Table of contents

SI 1. Experimental details

Materials: Lamotrigine, phenobarbital, dicarboxylic acids, and solvents were obtained from commercial suppliers and used without further purification.

Cocrystallization: All adducts were synthesized by liquid assisted grinding followed by slow evaporation method.

Lamotrigine-Phenobarbital cocrystal (LTG-PB): LTG-PB cocrystal was obtained by liquid assisted grinding method. Equimolar amount of LTG and PB (100-200 mg) were ground in a micro ball mill with 2-3 drops of methanol. The ground powder was dried overnight, recrystallized using methanol/acetonitrile mixture and left for slow evaporation at room temperature. Blocky colorless crystals were obtained in 4-5 days.

It is to be noted that neat grinding of two pure components resulted in an incomplete conversion i.e. mixture of cocrystal with parent drugs in the ground powder. The complete conversion of cocrystal was achieved on liquid assisted grinding.

LTG-PB cocrystal could be scaled up easily using solvent mediated transformation in which two compounds were mixed together with few drops of methanol and stirred in a sealed vial using a magnetic stir for 12 hours at 250 rpm. The resultant powder was dried and its phase purity was confirmed by PXRD.

Lamotrigine-Oxalic acid salt (LTG-OA): Both compounds (LTG and OA) in 1:2 molar ratios (100-200 mg) were ground with 3-4 drops of methanol in a micro ball mill (MillPrep™, quantochrome instruments). The ground powder was dried overnight, recrystallized using different solvents (methanol, ethanol, acetone, tetrahydrofuran, acetonitrile) and kept for slow evaporation at room temperature. Prism shaped crystals were obtained in 3-4 days. All solvents resulted in one crystal form only.

Lamotrigine-Malonic acid-tetrahydrofuran salt solvate (LTG-MA-THF): The salt was synthesized by grinding two components (1:2 molar ratios;100-200 mg) in a micro ball mill with 2-3 drops of THF. The powder was dried overnight and left for slow evaporation using THF. Blocky crystals were obtained in 2-3 days.

Lamotrigine-Sebacic acid salt (LTG-SA): Two compounds in equimolar ratios (100-200 mg) were ground in a micro ball mill using few drops of methanol. The powder was dried and recrystallized in methanol, ethanol, acetone etc. All solvents resulted in blocky crystals after 2-3 days.

Thermal analysis: DSC measurements of LTG, PB and LTG-PB cocrystal were performed on TA instruments Q20 DSC. Indium standard was used to calibrate the instrument and the samples were purged under nitrogen atmosphere. The measurements were conducted in hermitically sealed aluminum DSC pans at a heating rate of 10 °C/min from 30-400 °C. Thermograms were analyzed using TA Universal Analysis 2000, V 4.5A.

TGA of LTG-PB cocystal was collected on a TA Instruments Q50 thermogravimetric analyzer. The sample was heated in a platinum holder at a ramp rate of 10 °C/min from 30-400 °C under a N_2 atmosphere.

Raman spectroscopy: LTG-PB was analyzed by Raman spectroscopy using a Renishaw inVia Raman system equipped with a Leica microscope and a Rencam detector. A 633 laser with 1800 lines/nm grating and 50μm slit. The instrument was calibrated using a silicon standard in static mode. The spectra were collected in the range of 100-3500 cm^{-1} and analyzed using the WIRE 3.4 software package.

Powder X-ray diffraction: Powder X-ray diffraction patterns were collected on a Rigaku SmartLab diffractometer using Cu-Kα radiation (λ = 1.54187 Å), operating at 40 kV and 40 mA. The PXRD patterns were collected over 2θ range of 5°–50° with a step size of 0.01° and a step speed of 0.1 seconds. All powder patterns were processed using Jade 8 XRD Pattern Processing, Identification & Quantification analysis software (Materials Data, Inc.).[1]

Single crystal X-ray diffraction: Crystal structures of all the adducts were collected on a Rigaku AFC10K Saturn 944+ CCD-based X-ray diffractometer equipped with a low temperature device and Micromax-007HF Cu-target micro-focus rotating anode (λ = 1.54187 Å) operated at 1.2 kW power (40 kV, 30 mA). The X-ray intensities were measured at 85(2) K with the detector placed at a distance 42.00 mm from the crystal. Rigaku d*trek images were exported to CrysAlisPro for processing using CrystalClear 2.0 (Rigaku) and corrected for absorption. [2] The structure was solved and refined with the Bruker SHELXTL (version 2014/6)[3] software package. All non-hydrogen atoms were refined anisotropically with the hydrogen atoms placed in a combination of

idealized and refined positions. Full matrix least-squares refinement based on F^2 was used for all data.

Preparation of Simulated gastric fluid without pepsin (SGF): Sodium chloride (1.02 g) and 3.5 mL hydrochloric acid was dissolved in 500 mL deionized water at room temperature.

Preparation of Phosphate buffer saline (pH:7.2): Monosodium phosphate ($NaH_2PO_4.H_2O$, 0.584 g) and disodium phosphate ($Na_2HPO_4..7H_2O$, 1.547 g) were dissolved in 1L ionized water.

Intrinsic dissolution rate measurements: The μIDR™ miniature rotating disk method with the Pion Rainbow Dynamic Dissolution Monitor® system was used to collect the intrinsic dissolution rate (IDR) of LTG, PB and LTG-PB cocrystal. The calibration curves were made using standard solutions of known concentration for dissolution media (SGF and PBS). All the samples were pressed into pellets within metal disks using Pion μIDR press with a pressure of 150 psi for 5 minutes. The metal disks were submerged in 10 ml of dissolution media and were stirred at 250 rpm. UV-Vis probes with a path length of 2mm (for dissolution media: SGF) and 5mm (for dissolution media: PBS) were held above the disks. During dissolution experiments, 100 UV-Vis spectra were collected with 5 second interval followed by 200 spectra with 30 second interval at 37 ± 0.1 °C. As there was an overlap in the absorption spectra of two components in UV-Vis spectra, the concentrations of LTG and PB could not be measured directly using a single wavelength. Hence, the concentration of LTG and PB were calculated using following equation sets. The absorbance at two different wavelengths λ_1 and λ_2 have been used for calculation and these equations have been derived using Beer-Lambert law as follow:

$$A_{\lambda_1} = \sum_{i=1}^{N} \varepsilon_i c_i l$$

A dissolution system containing two different solutes at a specific time frames, could be expressed by two different absorption $A\lambda_1$ and $A\lambda_2$ and at wavelengths λ_1 and λ_2 as follow

$$A_{\lambda_1} = \varepsilon_{1\lambda_1} c_1 l + \varepsilon_{2\lambda_1} c_2 l = a_1 c_1 + a_2 c_2$$

$$A_{\lambda_2} = \varepsilon_{1\lambda_2} c_1 l + \varepsilon_{2\lambda_2} c_2 l = b_1 c_1 + b_2 c_2$$

Where a_1 and b_1 stands for absorbance of LTG solution with a unit concentration at wavelengths λ_1 and λ_2

a_2 and b_2 stands for absorbance of PB solution with a unit concentration at wavelengths λ_1 and λ_2. All these variables were calculated using standard calibration curve and the concentration of LTG and PB in solution c_1 and c_2 were expressed as

$$c_1 = \frac{a_2 A_{\lambda_2} - b_2 A_{\lambda_1}}{a_2 b_1 - a_1 b_2}$$

$$c_2 = \frac{b_1 A_{\lambda_1} - a_1 A_{\lambda_2}}{a_2 b_1 - a_1 b_2}$$

Therefore, the dissolution behavior of LTG/PB cocrystal can be described by the change in the concentration of LTG and PB in the dissolution media separately. The intrinsic dissolution rate was calculated by determining the slope of the initial linear region of the curve (concentration vs time profile) and then utilizing the slope (dc/dt) in the following equation:

$$IDR = V\frac{dc}{dt} * \frac{1}{Adisk}$$

where V= 10 mL and A_{disk} = 0.0707 cm^2.

The absorbance at 240 nm and 308 nm was selected for calculating LTG and PB concentration in PBS whereas in SGF, the absorbance at 240 nm and 280 nm were selected.

Cocrystal solubility measurements: Cocrystal equilibrium solubilities were measured in SGF and PBS at the eutectic point, where LTG and LTG-PB solid phases were in equilibrium with solution. This eutectic point was reached by suspending 200 mg of LTG-PB and 100 mg of LTG in 3 mL of media. Suspensions were continuously stirred at 27.5 ± 1.0°C. At 24 hour intervals, 0.50 mL aliquots of suspension were collected and filtered through a 0.45 μm pore membrane. The pH of the filtered solutions was measured before diluting with mobile phase and analyzing by HPLC. Solutions were considered to have reached equilibrium when less than 5% change in concentration was detected in both LTG and PB (48 – 72 h). The equilibrium solid phases were characterized by PXRD and DSC.

High-performance liquid chromatography (HPLC): Solution concentrations of LTG and PB were analyzed by Waters HPLC (Milford, MA) equipped with a UV/vis spectrometer detector. A reversed phase C18 Atlantis column (250 mm × 4.5mm i.d; 5μm) was maintained at 25 ± 1 °C and

used to separate LTG and PB. Injection volume was 20 µL and analysis was conducted using an isocratic method with a mobile phase composed of 55% methanol and 45% water with 0.1% trifluoroacetic acid and a flow rate of 1 mL/min. Absorbance of LTG was monitored at 266 nm and absorbance of PB was monitored at 230nm. The peak areas were integrated using Empower™ software program.

Cambridge Structural database (CSD) search: CSD analysis was performed using Conquest 1.19 with CSD version 5.38 (November 2016). Three different motifs; comprising only N···O homodimers, N···N homodimers and a heterodimer containing both N···O and N···N were used for the search. All the hydrogens were removed during the analysis. Intermolecular bonds were constrained to less than 4 Å, 3D coordinates defined for structures, organics only, no ions and intermolecular contacts. Rings were allowed for any substitution outside of the synthon contacts. The bond length in all the functionalities were averaged out and compared.

The analysis was performed using both room (273 K-303 K) and low (< 273K) temperature entries as shown in Figure 6 in manuscript. Then, it was repeated by restricting the entries to room temperature only, which also show the same trends (Figure S16).

SI 2. Characterization of LTG-PB cocrystal

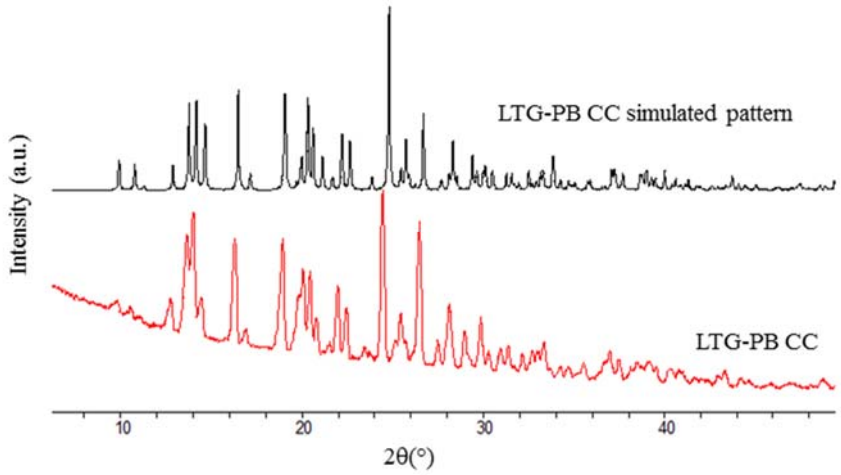

Figure S1. Experimental powder pattern of LTG-PB cocrystal in comparison to its simulated pattern.

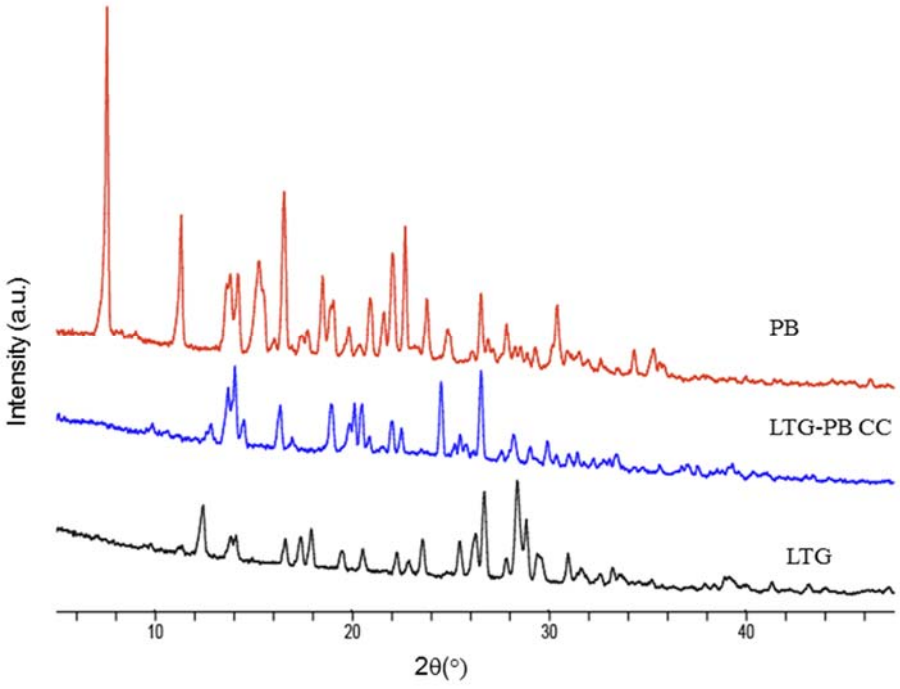

Figure S2. PXRD pattern of parent drugs (LTG and PB) and LTG-PB cocrystal.

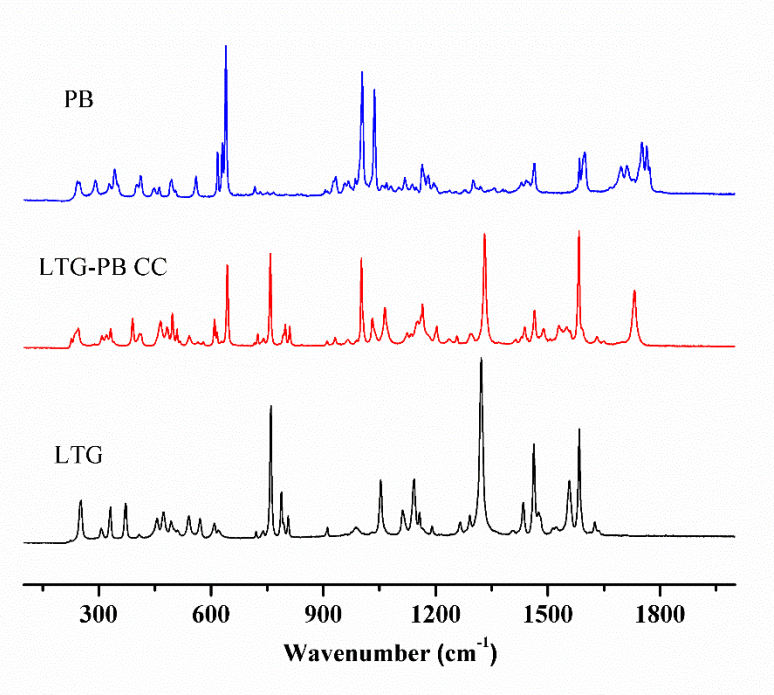

Figure S3. Raman spectra of parent drugs (LTG and PB) and LTG-PB cocrystal.

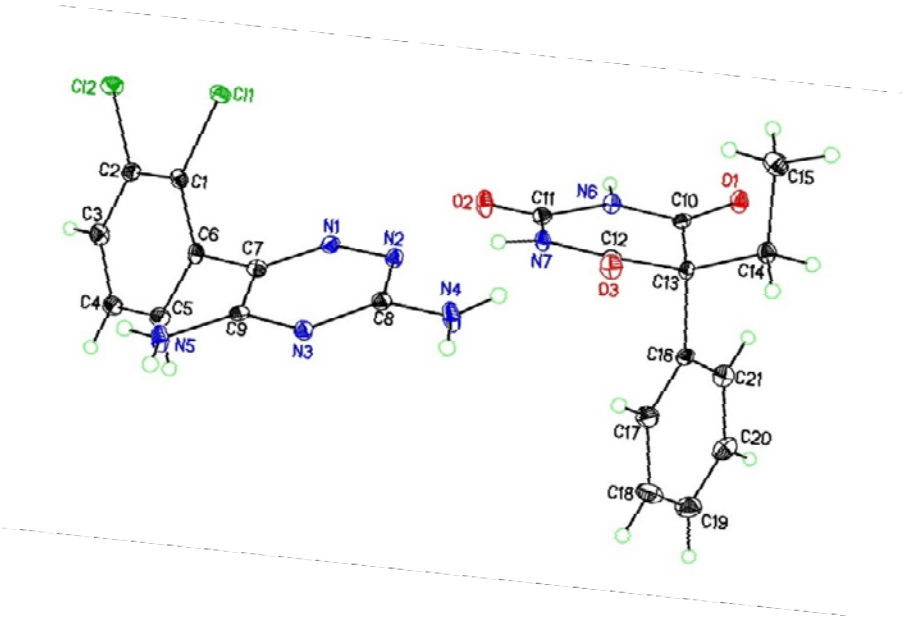

Figure S4. ORTEP diagram of the LTG-PB cocrystal (1:1 stoichiometry) collected at 85(2) K with thermal ellipsoids of 50% probability.

SI 3. Lamotrigine-dicarboxylic acids salts:

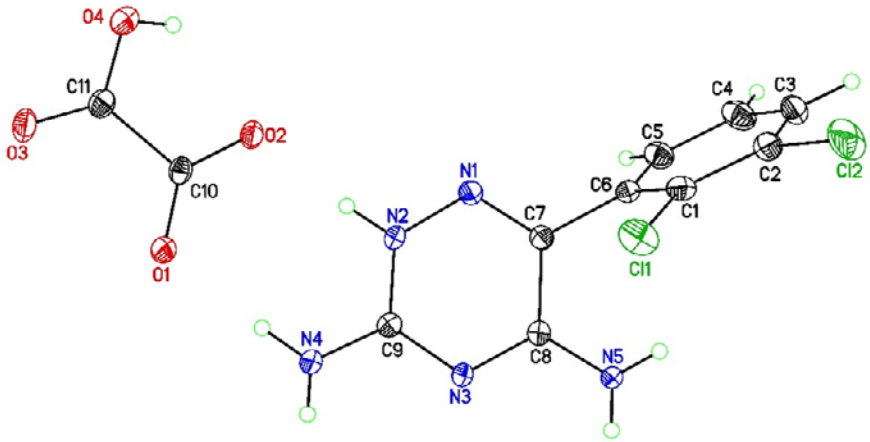

Figure S5. ORTEP diagram of the LTG-OA salt (1:1 stoichiometry) collected at 85(2) K with thermal ellipsoids of 50% probability.

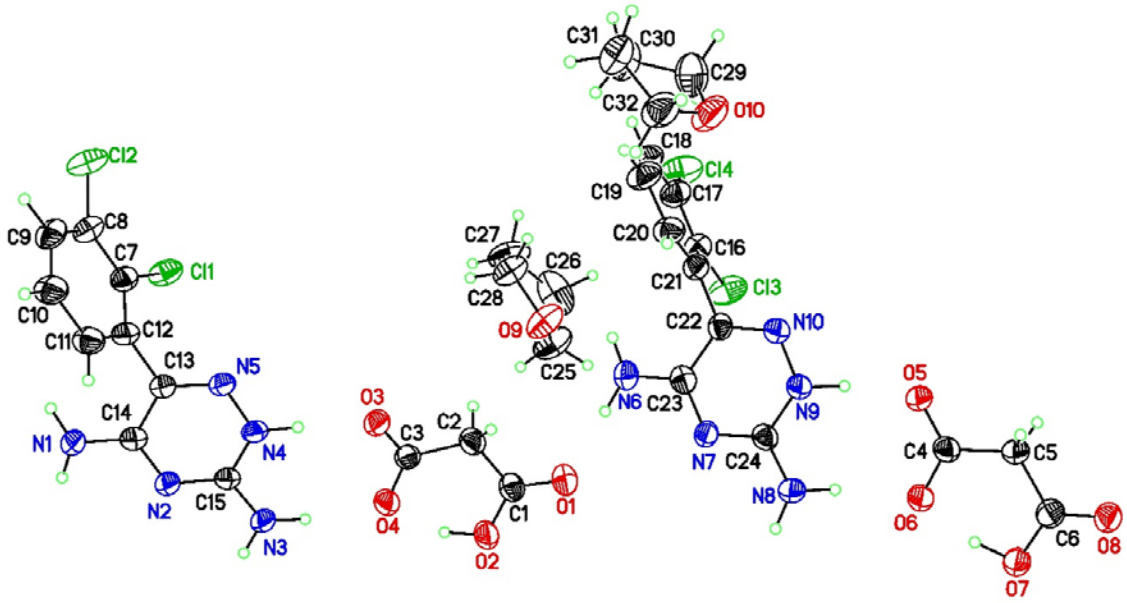

Figure S6. ORTEP diagram of the LTG-MA-THF salt solvate (2:2:1 stoichiometry) collected at 85(2) K with thermal ellipsoids of 50% probability.

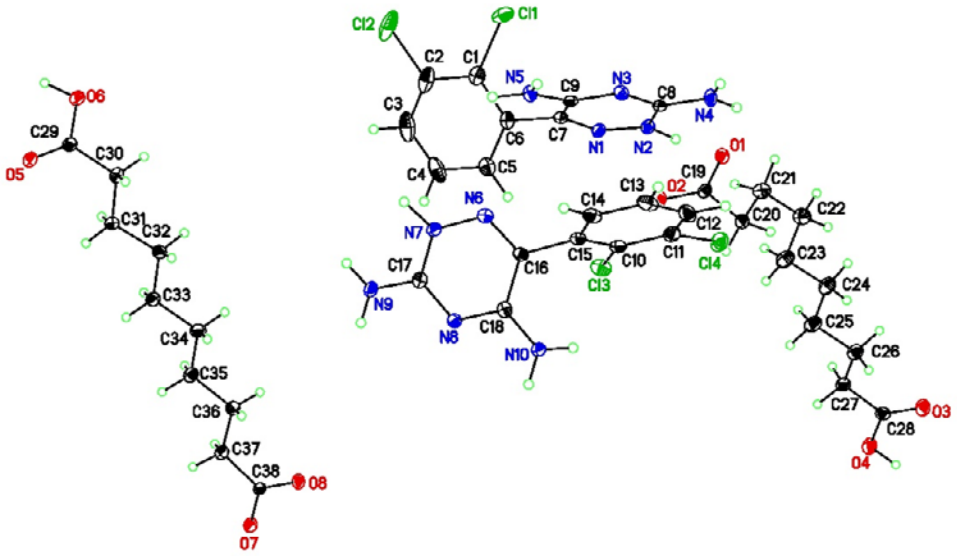

Figure S7. ORTEP diagram of the LTG-SA salt (2:2 stoichiometry) collected at 85(2) K with thermal ellipsoids of 50% probability.

Crystal Structural analysis:

The crystal structures of three novel salts between dicarboxylic acids and lamotrigine were elucidated. All salts display different hydrogen bonding features and crystal packing.

Lamotrigine-Oxalic acid salt (LTG-OA): Crystallization of a LTG and OA from methanol gave a salt with one molecule of LTG–H^+ and OA^- in an asymmetric unit (Figure S5). The crystal structure was solved and refined in the monoclinic system with $P2_1/c$ space group. Proton transfer from OA (O2) to the triazine moiety (N2) of LTG molecule was confirmed by equivalent carboxylate C–O^- bond lengths (1.259 Å and 1.237 Å). The crystal packing of the salt is sustained by both homodimer and heterodimer interactions. LTG and OA moieties interact via charge assisted hydrogen bonding N^+–H···O^- ($N2^+$–H2N···$O2^-$) and N4–H4B···O1 forming heterodimers between carboxylate and triazine/amino functionalities (shown in red highlight in Figure S8). These synthons are further connected by weak hydrogen bonds between the carboxylate on OA and additional amino groups on LTG. Amino/pyridine homodimers connecting the LTG (N5-H5C···N3, shown in blue highlight) extend the crystal packing into tapes (Figure S8).

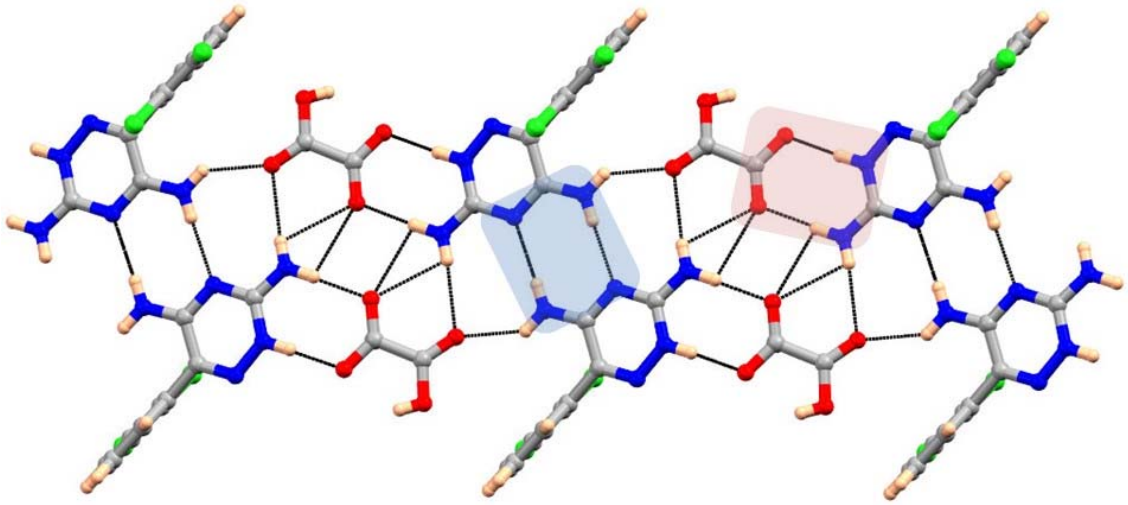

Figure S8. Hydrogen bonding features in LTG-OA salt. Both homodimers and heterodimers are shown in highlights.

Lamotrigine-Malonic acid-tetrahydrofuran salt solvate (LTG-MA-THF): This salt crystallizes in monoclinic system with non-centrosymmetric space group *Ia*. The asymmetric unit involves two LTG cations, two malonate anions, and two molecules of THF to form a salt solvate (Figure S6). Unlike LTG-OA, there are no homodimers present in this salt, and instead the structure is stabilized by heterodimer synthons formed between the amino/pyridinum and carboxylate moieties of LTG and MA via N^{+}-H···O^{-} hydrogen bonding. These dimers are further connected to an amino group of LTG which in turn interacts with the solvent molecule (THF) via N-H···O interactions (Figure S9). The crystal packing further extends in 3-dimension by bridging interactions between the carboxylate of malonic acid and chlorine on LTG.

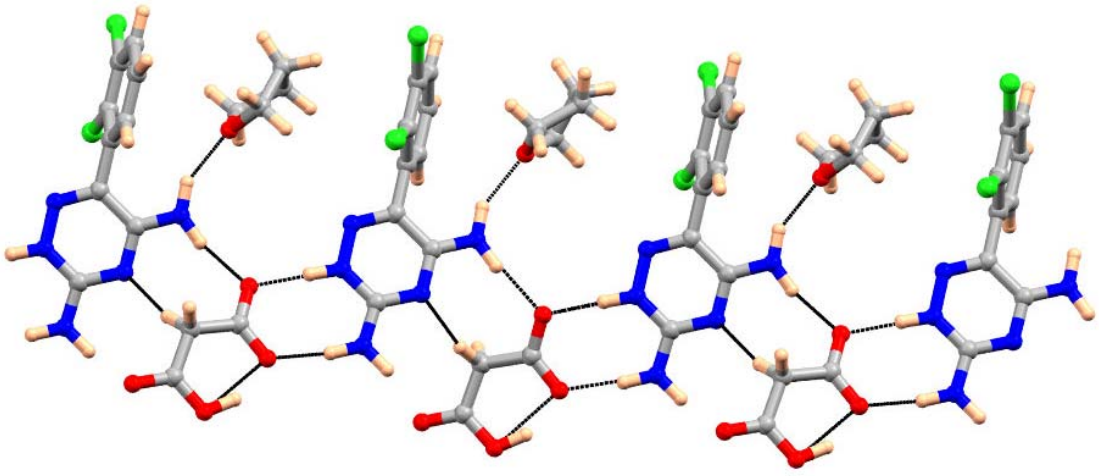

Figure S9. Hydrogen bonding features in LTG-MA-THF salt.

Lamotrigine-Sebacic acid salt (LTG-SA): This system crystallizes in non-centrosymmetric space group, *Pca*2_1 in orthorhombic system and contains two LTG cations and SA anions in an asymmetric unit (Figure S7). Here, amino/pyridine homodimer synthons are formed between symmetrical independent LTG molecules (red highlight in Figure S10). The amino group of two symmetrically independent LTG molecules further connects to carbonyl group of SA as shown in blue in Figure S10. Another motif comprises the charge assisted hydrogen bonding from N^+-H···O^- ($N2^+$-H2···$O1^-$), neutral N-H···O (N4-H4A···O5) and O-H···O(O6-H6···O1) with two symmetrically independent SA and LTG molecules, as shown in green in Figure S10. These interactions result in a zig-zag arrangement of LTG and SA molecules in 3-dimensions.

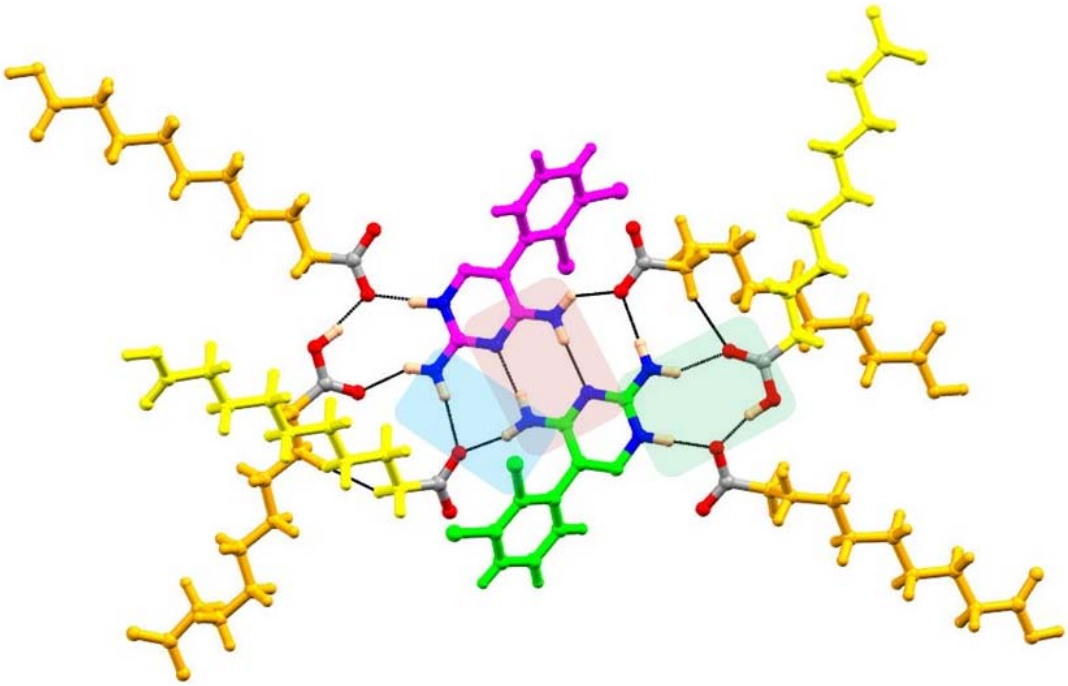

Figure S10. Hydrogen bonding features in LTG-SA salt. Symmetrically independent molecules are shown in different colors.

SI 4. Crystallographic parameter details

Table S1. Crystallographic details of cocrystals and salts reported in this study.

Data	LTG-PB	LTG-OA	LTG-MA	LTG-SA
Formula	$C_{21}H_{19}Cl_2N_7O_3$	$C_{11}H_9Cl_2N_5O_4$	$C_{16}H_{19}Cl_2N_5O_5$	$C_{19}H_{25}Cl_2N_5O_4$
Formula weight	488.33	346.13	432.26	458.34
Color	Colorless	Colorless	Colorless	Colorless
Crystal form	block	prism	block	block
CCDC number	1549455	1549452	1549453	1549454
Crystal size (mm)	0.19,0.14,0.14	0.24, 0.14, 0.14	0.28, 0.05, 0.04	0.23, 0.15, 0.13
Temperature (K)	85(2)	85(2)	85(2)	85(2)
Radiation	Cu Kα	Cu Kα	Cu Kα	Cu Kα
Wavelength (Å)	1.54187	1.54187	1.54187	1.54187
Crystal system	Monoclinic	Monoclinic	Monoclinic	Orthorhombic
Space group	*Cc*	$P2_1/c$	*Ia*	$Pca2_1$
a (Å)	7.4523(4)	11.5767(8)	22.4883(3)	14.6428(1)
b (Å)	17.8560(1)	12.2493(2)	10.6802(2)	7.7438(1)
c (Å)	16.4327(1)	9.9560(2)	16.8490(3)	38.5900(2)
α (°)	90	90	90	90
β (°)	92.48(1)	98.85(1)	99.73(2)	90
γ (°)	90	90	90	90
Volume ($Å^3$)	2184.60(2)	1395.03(11)	1629.90(6)	4375.75(5)
Z	4	4	8	8
Density (gcm^{-3})	1.485	1.648	1.440	1.391
Absorption coefficient (mm^{-1})	3.022	4.460	3.273	2.977
F (000)	1008	704	1792	1920
$\theta_{min, max}$	4.954, 69.264	3.60, 68.30	3.989, 69.369	4.583, 69.394
No. Unique Reflns.	3497	2534	6887	8083
No. of parameters	324	224	553	591
$h_{max, min}$	9, -8	13, -13	27, -27	17, -17
$k_{max, min}$	21, -21	14, -13	12, -12	9, -9
$l_{max, min}$	19, -19	11, -11	20, -20	46, -46
$R_{\_all}$, $wR2_{\_all}$	0.0227, 0.0586	0.0381, 0.0945	0.0634, 0.1605	0.0377, 0.0970
$R_{\_obs}$, $wR2_{\_obs}$	0.0227, 0.0586	0.0378, 0.0942	0.0590, 0.1529	0.0376, 0.0970
$\Delta\rho_{min}$, $\Delta\rho_{max}$ ($eÅ^{-3}$)	0.214, -0.244	0.413, -0.404	0.673, -0.371	0.733, -0.351
GooF	1.126	1.099	1.027	1.120

SI 5. Dissolution profile of LTG-PB cocrystal

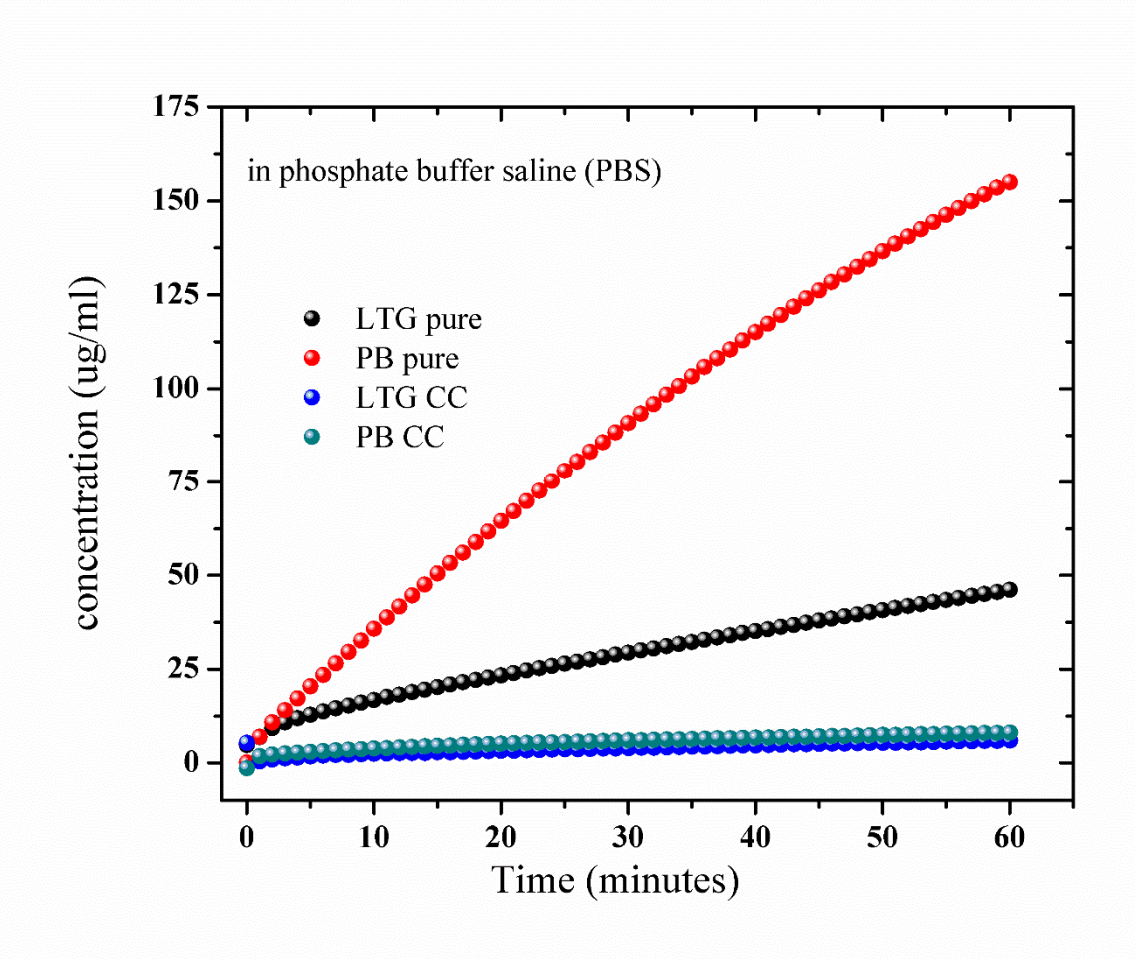

Figure S11. LTG-PB cocrystal and parent drugs dissolution profile in phosphate buffer saline.

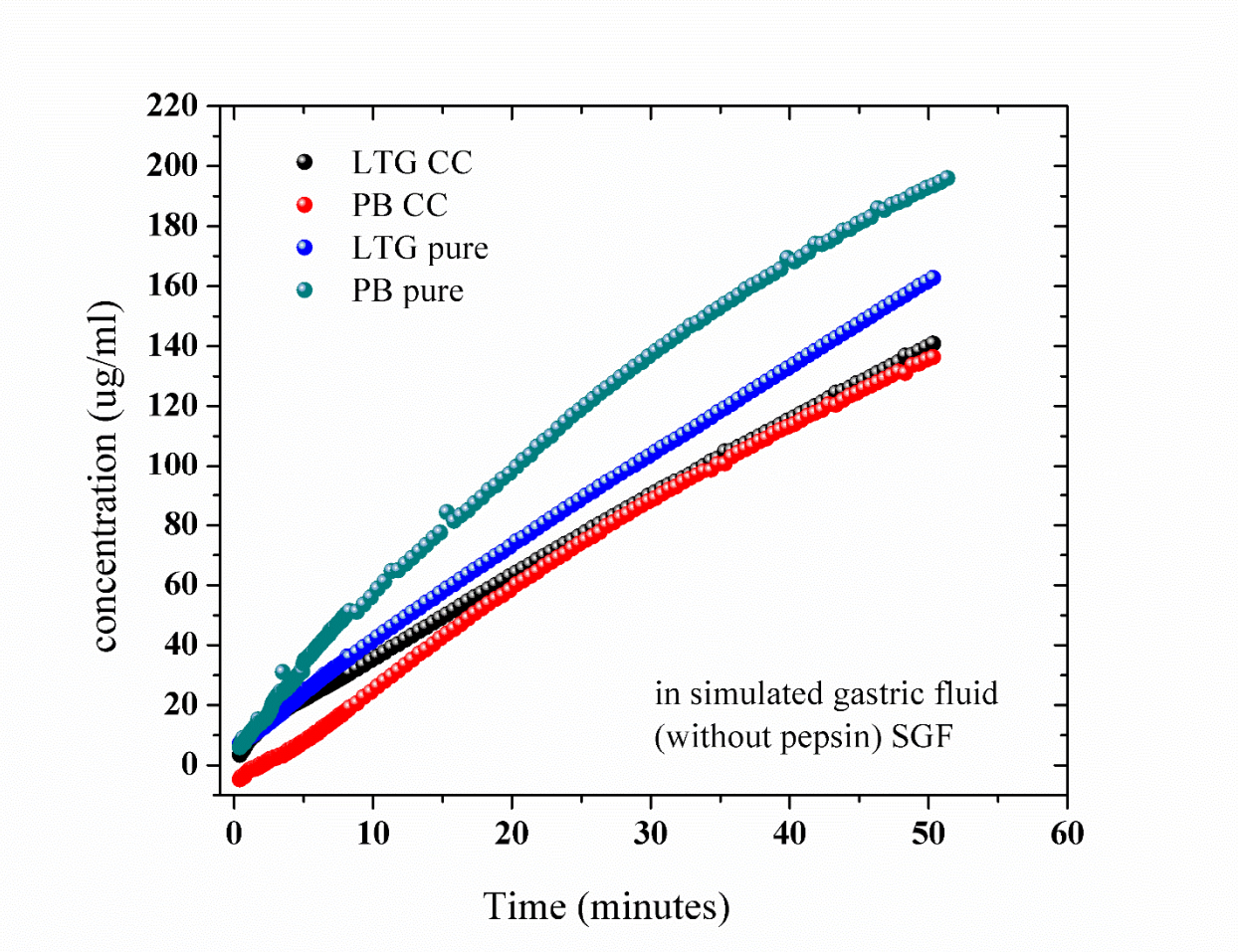

Figure S12. LTG-PB cocrystal and parent drugs dissolution profile in simulated gastric fluid.

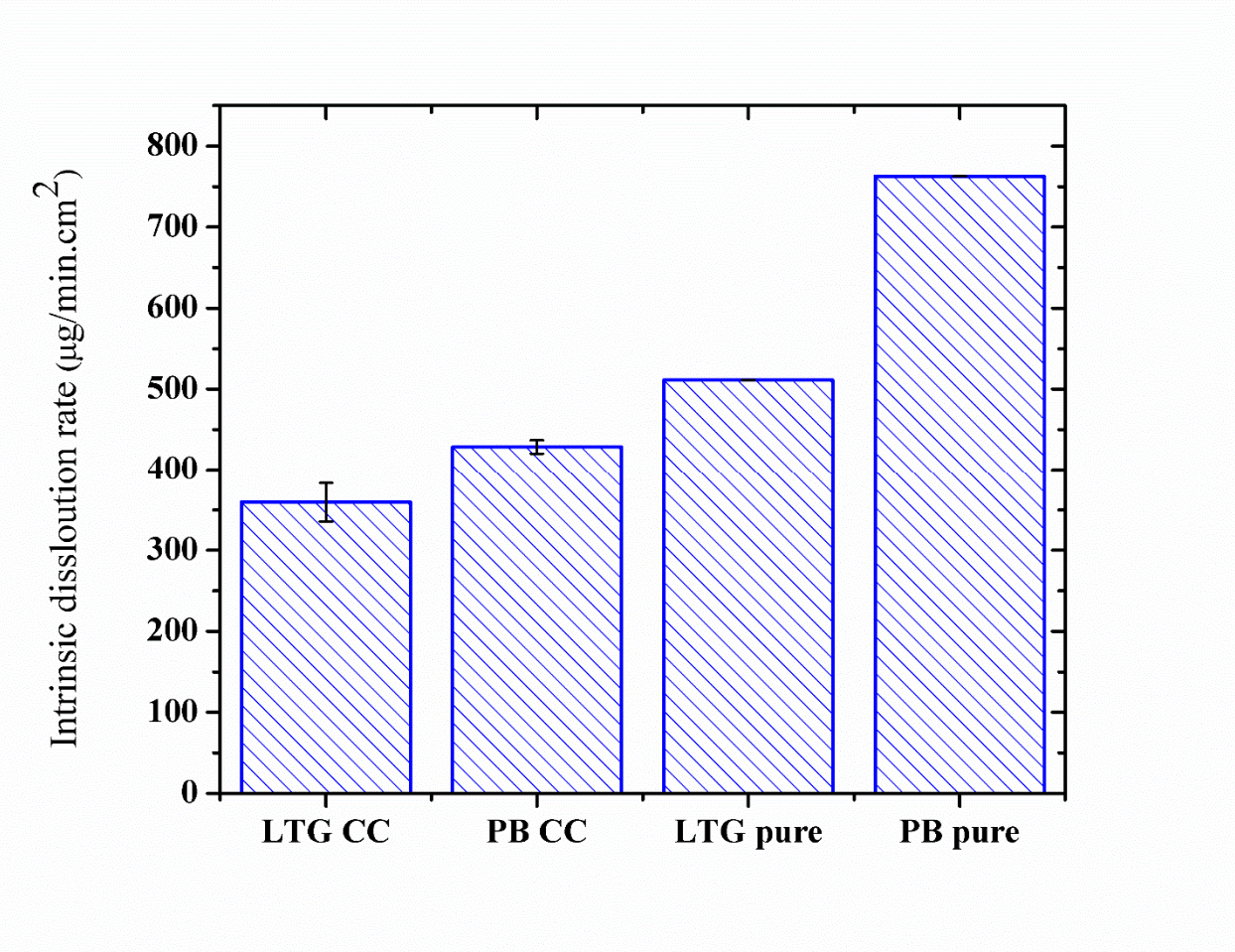

Figure S13. Intrinsic dissolution rate of LTG and PB from single component crystals and a newly discovered cocrystal at 37± 0.1 °C in simulated gastric fluid.

SI 6. Powder X-ray diffraction of LTG-PB cocrystal after dissolution

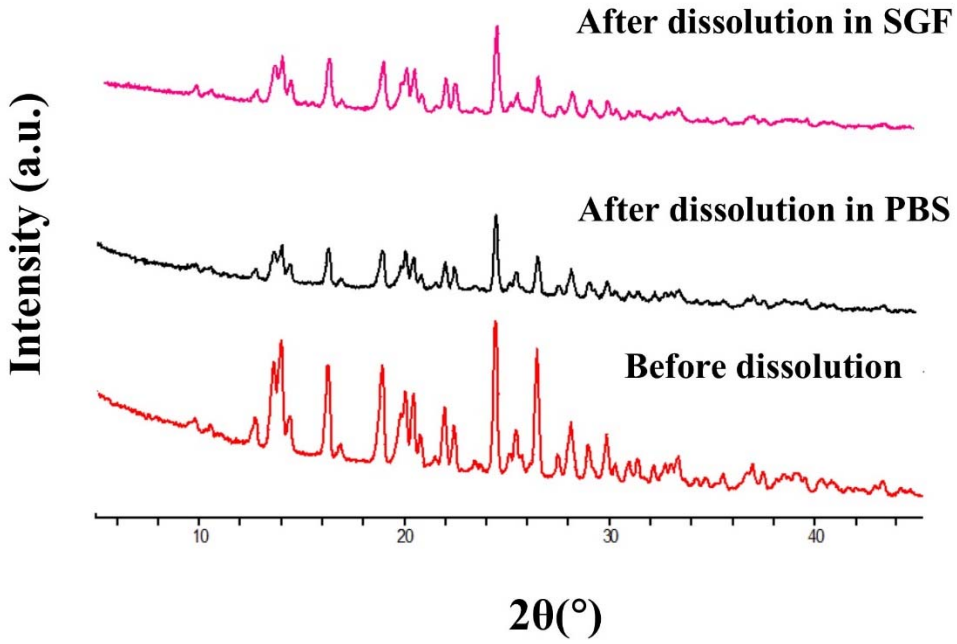

Figure S14. PXRD pattern of LTG-PB cocrystal obtained after dissolution in PBS and SGF showed complete match with the PXRD pattern collected before dissolution on cocrystal.

SI 7. Cocrystal solubility measurements

LTG is a weak base, and its solubility dependence on pH was previously described by

$$S_{LTG} = S_{LTG,0}(1 + 10^{pKa,LTG-pH}) \quad (1)$$

where $S_{LTG,0}$ represents the solubility of LTG under nonionizing conditions, or intrinsic drug solubility.[4] $S_{LTG,0}$ has been found to be 6.6 x 10^{-4} M. PB is a diprotic acidic drug with $pK_{a,1}$ of 7.46 and $pK_{a,2}$ 11.8.[5] PB solubility as a function of pH is

$$S_{PB} = S_{PB,0}(1 + 10^{pH-pKa,PB1} + 10^{2pH-pKa1,PB-pKa2,PB}) \quad (2)$$

where $S_{PB,0}$ represents the intrinsic solubility of PB. $S_{PB,0}$ was obtained from the above equation and found to be 4.3 x 10^{-3} M.

Cocrystal solubility is the sum of all cocrystal component species in solution that are in equilibrium with the cocrystal. An expression that relates cocrystal solubility with pH was obtained by considering the equilibrium of cocrystal dissociation defined by the solubility product K_{sp} and the equilibria of the cocrystal component ionizations defined by their respective ionization constants K_a. The cocrystal solubility dependence of pH is

$$S_{LTG-PB} = \sqrt{K_{sp}(1 + 10^{pKa,LTG-pH})(1 + 10^{pH-pKa1,PB} + 10^{2pH-pKa,PB1-pKa2,PB})} \quad (3)$$

Full derivation of the cocrystal solubility equation has been previously presented.[4b,6] K_{sp} in Table S2 was obtained from the above equation from experimental measurements of S_{LTG-PB} at a given pH.

Table S2. K_{sp} and pH_{max} values in LTG-PB cocrystal

Cocrystal	K_{sp} (M^2)	pH_{max} (PB and LTG-PB)	pH_{max} (LTG and LTG-PB)
LTG-PB	(1.2 ± 0.1) x 10^{-8}	2.6	9.0

The 1:1 cocrystal stoichiometric solubility was calculated according to

$$S_{LTG-PB} = \sqrt{[LTG]_{T.eu}[PB]_{T,eu}}$$

from measured total eutectic concentrations of LTG and PB ($[LTG]_{T,eu}$ and $[PB]_{T.eu}$) shown in Table S3.[4,7]

Table S3. Characterization of cocrystal and drug eutectic points in SGF and PBS: solution pH, eutectic concentration of LTG and PB, and solid phases.

	Initial pH	**Final pH**	**LTG (mM)**	**PB (mM)**	**Initial Solid Phases**	**Final Solid Phases**
SGF	1.18	4.26	13.5 ± 0.3	(1.57 ± 0.09) x 10^{-2}	LTG and LTG-PB	LTG and LTG-PB
PBS	7.28	7.23	0.90 ± 0.04	(29.4 ± 1.5) x10^{-2}	LTG and LTG-PB	LTG and LTG-PB

SI 8. DSC plot of LTG and PB drugs

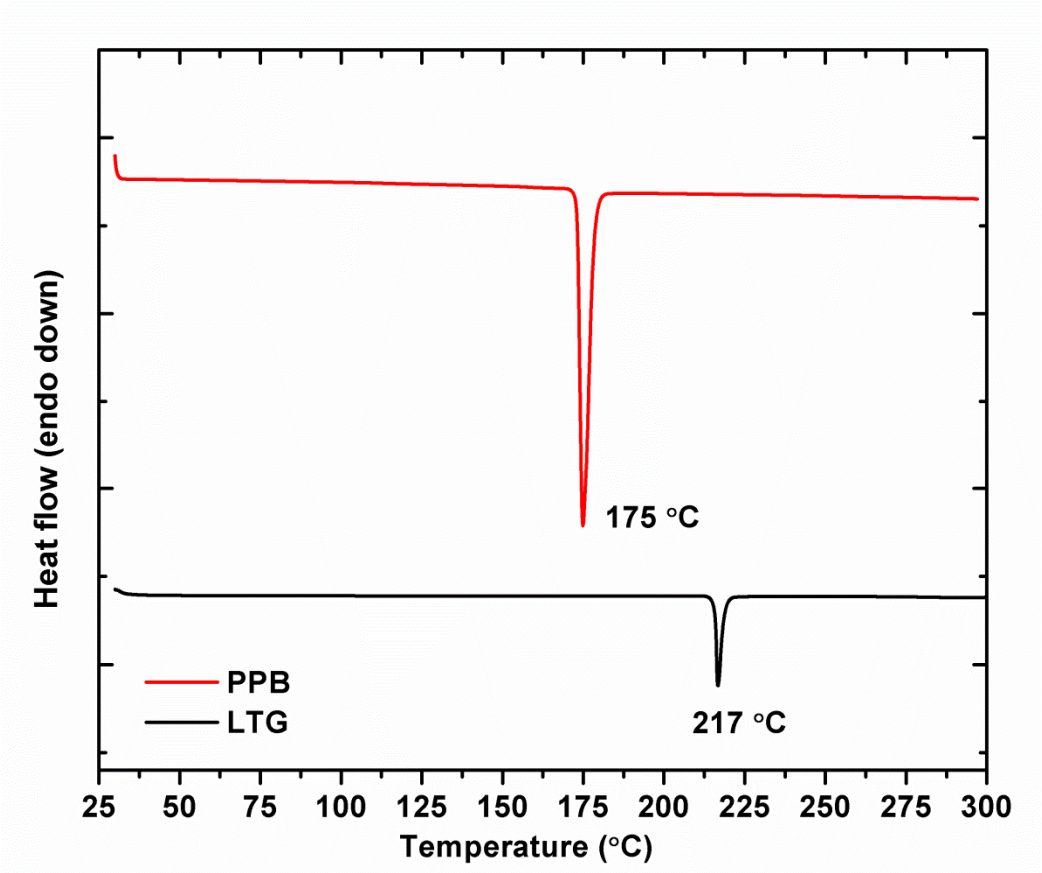

Figure S15. DSC plot of LTG and PB showing their melting points.

SI 9. Cambridge Structural Database analysis:

CSD analysis was performed as mentioned in the experimental section. A total of 1151 hits were found for pyridine/amino (N···N homodimers), whereas amino/carbonyl (O···N homodimers) showed 477 hits including both room and low temperature. The hits for all temperature range (room to low temperature) were found to be 21 for both N···N and O···N heterodimers. Average intermolecular bond lengths in pyridine/amino homodimer, amino/carbonyl homodimer, and the heterodimer formed by both functionalities with standard deviation of the mean were plotted as shown in Figure 6 in manuscript.

The data, which was used to create bar graph at all temperature range (Figure 6) and only room temperature (Figure S16), are given in Table S4 and S5 respectively.

Table S4. Details of CSD analysis at both room and low temperature.

	N···N		**O···N**	
	homodimers	**heterodimers**	**homodimers**	**heterodimers**
Average bond distance (Å)	3.365	3.180	3.217	3.023
Standard error	0.010	0.045	0.018	0.059
Number of hits	1151	21	477	21

Table S5. Details of CSD analysis at room temperature.

	N···N		**O···N**	
	homodimers	**heterodimers**	**homodimers**	**heterodimers**
Average bond distance (Å)	3.361	3.088	3.207	2.936
Standard error	0.016	0	0.022	0.005
Number of hits	508	2	271	2

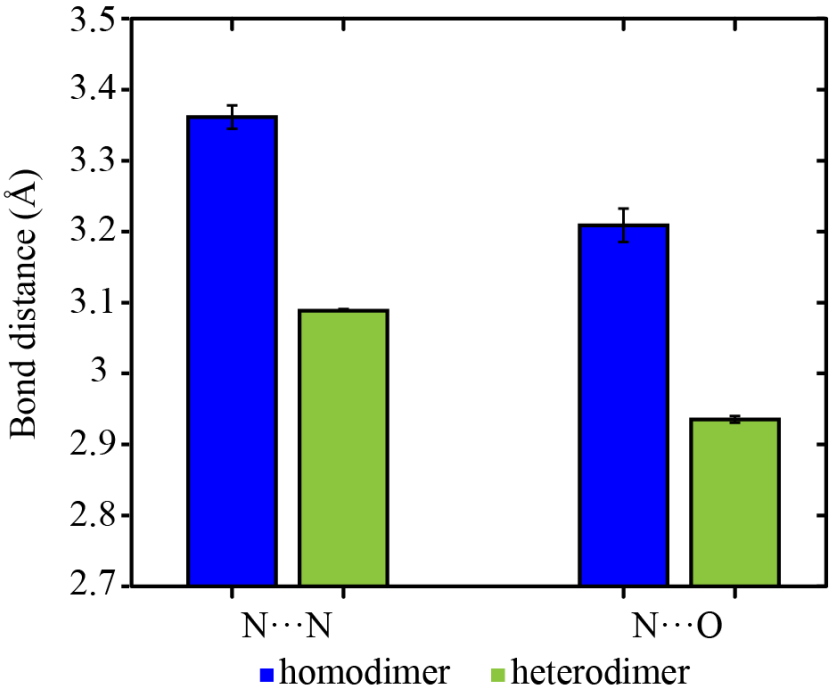

Figure S16. Average intermolecular bond lengths in pyridine/amino homodimer, amino/carbonyl homodimer, and the heterodimer formed by both functionalities in CSD at room temperature. Error bars show standard deviation of the mean.

SI 10. References

1. Jade Plus 8.2 ed.; Materials Data, Inc. 1995-2007.
2. CrystalClear Expert 2.0 r16, Rigaku Americas and Rigaku Corporation (2014), Rigaku Americas, 9009, TX, USA 77381-5209, Rigaku Tokyo, 196-8666, Japan. CrysAlisPro 1.171.38.41 (Rigaku Oxford Diffraction, 2015).
3. Sheldrick, G.M. SHELXTL, v. 2014/6; Bruker Analytical X-ray, Madison, WI, 2014.
4. (a) Maheshwari, C.; University of Michigan. Library. Deep Blue., Understanding the Solution Phase Chemistry and Solid State Thermodynamic Behavior of Pharmaceutical Cocrystals. 2012. http://hdl.handle.net/2027.42/96113; (b) Kuminek, G.; Rodriguez-Hornedo, N.; Siedler, S.; Rocha, H. V.; Cuffini, S. L.; Cardoso, S. G. *Chem. Commun.* **2016**, *52*, 5832-5.
5. (a) Geiser, L.; Henchoz, Y.; Galland, A.; Carrupt, P. A.; Veuthey, J. L. *J. Sep. Sci.* **2005**, *28*, 2374-2380; (b) O'Neil, M.J.; Smith, A.; Heckelman, P.E. The Merck Index: an encyclopedia of chemicals, drugs, and biologicals. Whitehouse Station: NJ, 2001; Vol. 13th edn.
6. Bethune, S. J.; Huang, N.; Jayasankar, A.; Rodriguez-Hornedo, N. *Cryst. Growth Des.* **2009**, *9*, 3976-3988.
7. (a) Maheshwari, C.; Andre, V.; Reddy, S.; Roy, L.; Duarte, T.; Rodrigez-Hornedo, N. *Crystengcomm* **2012**, *14*, 4801-4811; (b) Good, D. J.; Rodriguez-Hornedo, N. *Cryst. Growth Des.* **2009**, *9*, 2252-2264.